SLOWED ROTOR WIND TUNNEL TESTING OF AN INSTRUMENTED ROTOR AT HIGH ADVANCE RATIO

Ben Berry
Graduate Research Assistant

Inderjit Chopra
Alfred Gessow Professor and Director

Alfred Gessow Rotorcraft Center
Aerospace Engineering, University of Maryland
College Park, MD, 20742, U.S.A.

Compound helicopter designs utilize a slowed main rotor, which reduces RPM as flight speed increases to maintain sub-critical tip Mach numbers. These concepts are therefore expected to operate at high advance ratios (1–2.5 or higher). There is a need for experimental data sets in this flight regime to validate and develop predictive tools. Systematic testing in the Glenn L. Martin Wind Tunnel (University of Maryland) was conducted on an instrumented Mach-scale articulated rotor (1.7 m diameter) up to an advance ratio of 1.61. The following measurements were taken: steady and dynamic 6-component hub loads (fixed-frame), shaft torque (rotating frame), root flapping angles, pitch link loads, blade torsion and flap bending moments at 5 spanwise stations, and 16 chordwise blade pressures at 30% radius spanwise location. The selected results detailed in this paper revealed insights into high advance ratio, reverse flow phenomenon such as reverse chord dynamic stall and the resulting impact on loads. The combination of rotor advance ratios beyond 1.0, large collective pitch sweeps, and blade surface pressure measurements makes this data set unique.

1. NOTATION

np	n/rev, frequency normalized by rotor rotational speed
a	Speed of sound
c	Rotor blade chord, 8.0 cm (3.15 in)
D	Rotor drag, wind-axis
D_E	Rotor equivalent drag = P/V+D
C_{DE}	Equivalent drag coefficient, $C_P/\mu+C_D$
C_H	Rotor H-force, non-dim by $\rho\pi R^2(\Omega R)^2$
C_T	Rotor thrust, non-dim by $\rho\pi R^2(\Omega R)^2$
C_Y	Rotor side force, non-dim by $\rho\pi R^2(\Omega R)^2$
C_{RM}	Rotor rolling moment, non-dim by $\rho\pi R^2(\Omega R)^2 R$
C_{PM}	Rotor pitching moment, non-dim by $\rho\pi R^2(\Omega R)^2 R$
C_P	Power coefficient = $P/\rho\pi R^2(\Omega R)^3$
F_X, H	Hub axial force, positive aft
F_Y, Y	Hub side force, positive starboard (advancing side)
F_Z, T	Hub vertical force (thrust), positive up
L	Rotor lift, wind-axis
LE	Airfoil leading edge
M	Local Mach number
M^2C_p	Pressure coefficient, $(p-p_\infty)/(1/2\rho a^2)$
M^2c_c	Chord force, non-dim by $1/2\rho a^2 c$
M^2c_m	Pitching moment at c/4, non-dim by $1/2\rho a^2 c^2$
M^2c_n	Normal force, non-dim by $1/2\rho a^2 c$
P	Rotor shaft power
p	Blade surface pressure
p_∞	Freestream pressure
R	Rotor radius, 0.849 m (2.79 ft)
TE	Airfoil trailing edge
TPP	Rotor tip path plane
V	Tunnel freestream velocity
X	Rotor propulsive force = -D
α_s	Longitudinal shaft tilt, positive nose up
β_{1c}	1p longitudinal root flapping amplitude
β_{1s}	1p lateral root flapping amplitude
μ	Advance ratio, $V/\Omega R$
ρ	Freestream density
σ	Rotor solidity, 0.12
θ_{1c}	Lateral cyclic, deg
θ_{1s}	Longitudinal cyclic, deg
θ_0	Root collective angle, deg
Ω	Rotor angular velocity, positive CCW

2. INTRODUCTION

The motivation of this work is to investigate the aeromechanics of high-advance ratio edgewise rotors. The primary approach is to create a high-quality experimental data set, which can be used to explore the physics of this flight regime and validate predictive tools for next-generation compound rotorcraft.

A central feature of future high-speed compound rotorcraft concepts is a slowed main rotor, where the

Presented at the 40th European Rotorcraft Forum, Southampton, England, September 2–5, 2014.

rotor speed is reduced as the aircraft speed increases. This is done typically to maintain a sub-critical advancing tip Mach number and reduce profile power. Slowed-rotor compounds are expected to operate at high advance ratios (1–2.5 or higher). As a result, the entire retreating blade will be operating in a reverse-flow condition. Predictive tools (both comprehensive analysis and CFD/CSD coupled analysis) have not been extensively validated in this operating regime due to a dearth of experimental data.

Testing in the Glenn L. Martin Wind Tunnel at the University of Maryland (UMD) was conducted with the goal of creating publicly available data sets to benchmark analyses, and to enhance fundamental understanding of the aeromechanics in this unique flight regime.

2.1 Relevant Prior Work

In the late 1960's there were several high advance ratio rotor wind tunnel tests which are commonly cited and used for predictive validation. Jenkins[1] tested a 15-ft diameter model rotor to advance ratios up to 1.45. This was the first work to experimentally observe the collective-thrust control reversal phenomenon, as well as provide thrust, torque, and H-force data. Explanations of the collective-thrust reversal are given in Ref 2–5. Floros and Johnson[6] performed correlation of CAMRAD II analysis with the Jenkins data set, with good agreement of thrust trends. Several full-scale rotor geometries were wind tunnel tested to high-advance ratio and reported by McCloud and Biggers in 1968[7], with performance measurements taken up to a maximum advance ratio of 1.05. These test data were compiled and analyzed by Harris[3] and Ormiston[4], with comparisons to predictive methods. The most recent high-advance ratio test was the full-scale UH-60A airloads rotor, tested in the U.S. Air Force's NFAC facility at NASA Ames Research Center[8]. Slowed-rotor conditions up to advance ratio of 1.0 were explored, and a comprehensive set of measurements were taken, including blade pressures at several stations. Analysis of select data from this test were reported by Datta, Yeo, and Norman in Ref 9–11.

The first phase of high μ testing at UMD in 2009 reached advance ratios of 0.66 while investigating the effect of variable RPM on performance and loads[12]. The second phase of testing in 2011 achieved advance ratios of 1.2 and focused on conditions for compound helicopters, such as rearward shaft tilt[5]. Testing was conducted in 2012 up to advance ratio of 1.0 on different rotor geometry and compared results with previous testing for performance and vibratory loading trends[13]. The most recent test entry in 2013 reached advance ratios of 1.41, but points beyond 1.04 were only taken at zero collective pitch[14]. The 2013 test was also the first at UMD to incorporate pressure transducers within the blade surface. However, nearly all of the pressure sensors aft of the 0.25c position failed early in testing, which eliminated the possibility of integrating sectional airloads, or even the observation of possible trailing edge suction peaks in reverse flow. Based on the lessons learned from previous testing, the experiment introduced in this paper addressed many of these deficiencies.

3. EXPERIMENTAL SETUP

Testing was performed on a 5.6 ft (1.7 m) diameter model rotor using a Mach-scale fully articulated rotor test stand. The test was conducted in the Glenn L. Martin Wind Tunnel. It is a closed circuit tunnel with a rectangular test section 11 ft (3.35 m) wide and 7.75 ft (2.36 m) tall. The maximum wind speed capability is 200 kts (370 km/h), which is approximately a freestream Mach number of 0.3. The maximum wind speed reached in this test was 125 kts (230 km/h). The model rotor setup installed in the wind tunnel is shown in Figure 1. A fuselage-shaped fairing was not used in an attempt to mimic an isolated rotor for ease of analysis correlation. Tunnel wall corrections were not applied to the measurements.

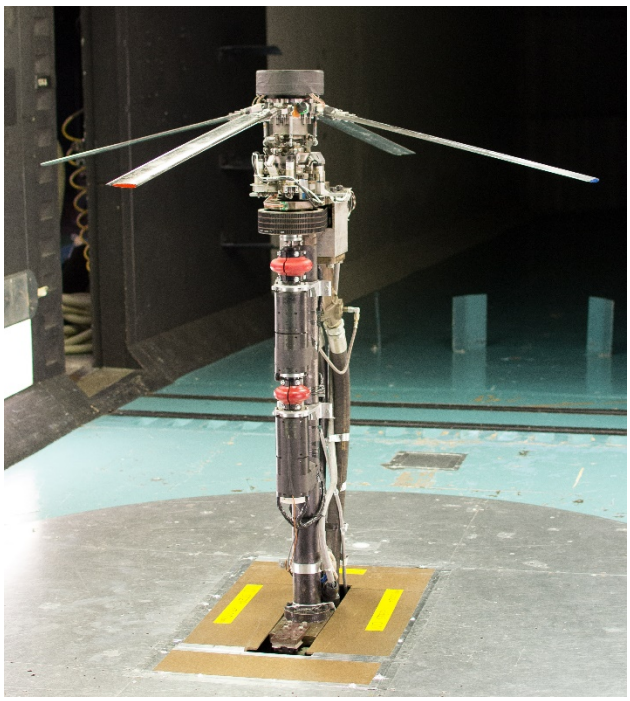

Figure 1: Rotor test stand installed in the Glenn L. Martin Wind Tunnel

3.1 Instrumentation and Equipment

3.1.1 Rotor Hub and Stand

The rotor hub is a fully-articulated hub with coincident flap and lag hinges at 0.063R offset. Rotor power was supplied by a 75 hp hydraulic motor with a 2:1 reduction belt drive system. The rotor pulley is connected to the rotor shaft through a splined gear. The rotor shaft is connected to the rotor hub through a shear disk, which is instrumented to give rotating shaft torque. The splined gear provides a vertically floating attachment to the entire rotor hub, which is supported by the fixed-frame rotor balance. The strain-gaged fixed-frame rotor balance load cell provides static and dynamic signals of five-components (the sixth, yaw moment, is not used). Static and dynamic calibrations of the rotor balance are described in later sections of this paper. The balance also supports the non-rotating swashplate actuators, which are electric motors geared to a leadscrew. The linear travel of each actuator is separately measured by linear travel sensors (linear variable differential transformers), which, when calibrated, give the collective, longitudinal cyclic, and lateral cyclic settings of the rotor.

A toothed-wheel connected to the rotor pulley and an optical sensor give 60/rev and 1/rev signals for calculating rotor RPM and azimuthal referencing. There is an additional rotary hall-effect IC sensor that outputs voltage proportional to azimuth position.

The rotating sensor signals (shaft torque and the rotor blade instrumentation) were passed through the hollow rotor shaft to the two sliprings that were mounted below the rotor pulley through a flexible coupling. The sliprings were designed and manufactured by Fabricast, and each had 64 rings with 28 gage (AWG) flying lead wires.

A three-axis, 6g accelerometer was mounted on the rotor stand (non-rotating) to monitor stand vibrations during testing and as a check for fixed-frame vibratory load trends.

3.1.2 Data Acquisition

All signals were recorded at a 5 kHz sampling rate using a National Instruments 16-bit ADC. Each flight condition was recorded for 10 seconds. Strain gage and pressure sensor signals were processed through SCXI-1520 modules using a 1 kHz low-pass filter (3rd order Butterworth). High-level voltage signals (flap hinges, shaft encoder, accelerometer, swashplate orientation) were processed through SCXI-1102C modules. A LabVIEW virtual instrument panel was programmed for monitoring select signals for rotor operation/trimming, safety of flight, and for data file recording.

3.1.3 Rotor Blade Properties

The rotor blades were constructed in-house from a Rohacell 31 foam core, an IM8 (Patz resin) unidirectional carbon rectangular spar, and a single ply of 0-90 fiberglass prepreg. A separate outer skin was pre-cured separately out of IM7/8552 plain weave prepreg with +/-45 degree orientation. This was done to allow embedding of the sensors under the surface before the final skin cure at room temperature. Tungsten-carbide rods (9/64" diameter) were embedded as leading-edge weights for CG balance. The nominal rotor properties are listed in Table 1.

Table 1: Rotor properties

Number of blades	4
Radius, ft (m)	2.79 (0.849)
Chord, in (cm)	3.15 (8.0)
Solidity	0.120
Lock No.	5.5
Airfoil section	NACA 0012
100% RPM	2300
Tip speed, ft/s (m/s)	675 (206)
Tip Mach	0.60
Tip Reynolds	1.1×10^6
Hinge offset	6.3%
Root cutout	22.3%

Two of the four rotor blades contained embedded instrumentation. Blade #3 was instrumented with 12 full-bridge strain gages to measure blade loads. Flap-wise bending moment and torsion moment bridges were placed at 30, 40, 50, 60, 70, and 90% radial locations. The gages at 0.9R exhibited unacceptable errors during the calibration phase, and were not used.

Blade #1 contained embedded pressure transducers in a chordwise arrangement at a single radial station, 0.3R (Table 2). This station was chosen to investigate the impact of high reverse-flow velocities while maintaining distance from blade root effects. Figure 3 shows a sketch of the size and location of the embedded transducers in the rotor blade airfoil.

The pressure transducers were model 40931 silicon MEMS sensors from Meggitt Sensing System's Endevco product line, with a 0–15 psia full-scale range and stated resonance frequency of 180 kHz. The sensor was supplied in a die form (no packaging) with surface mounting pads. Due to the miniature size of the sensor (1.65 x 1.2 x 0.4 mm) a custom printed circuit board was designed to serve

as a “breakout board” for attachment of lead wiring (Figure 4).

The dynamic response of the Endevco sensors was verified experimentally up to the maximum frequency of interest for this experiment (200 Hz, >12/rev). Higher frequencies were not verified due to testing limitations. The average transverse acceleration sensitivity for the installed transducers was measured as 0.000207 psi/g (3.00E-05 kPa/g).

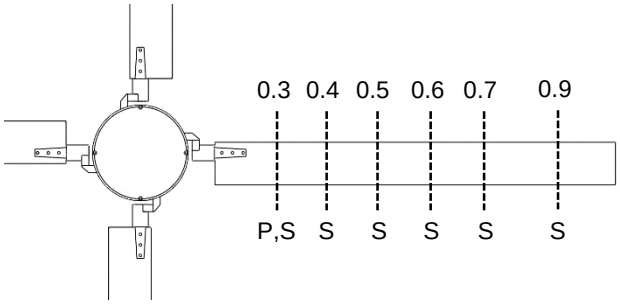

Figure 2: Top-view schematic of rotor showing radial locations of pressure transducers (Blade 1, “P”) and flap bending & torsion strain gages (Blade 3, “S”).

Table 2: Non-dimensional chordwise distribution of the 19 blade pressure transducers (0.3R station, blade #1). Highlighted sensors were not functional for the entire testing program.

	Upper surface (x/c)	Lower surface (x/c)
1	0.029	0.029
2	0.076	0.076
3	0.127	0.127
4	0.190	0.190
5	0.317	0.317
6	0.460	0.460
7	0.603	0.603
8	0.730	0.730
9	0.829	0.790
10	-	0.879

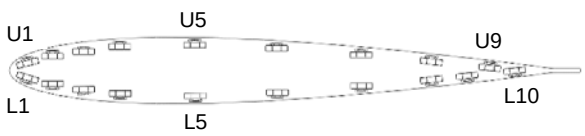

Figure 3: Airfoil cross-section (3.15”, 8.0 cm total chord length) showing chordwise placement of embedded pressure transducers.

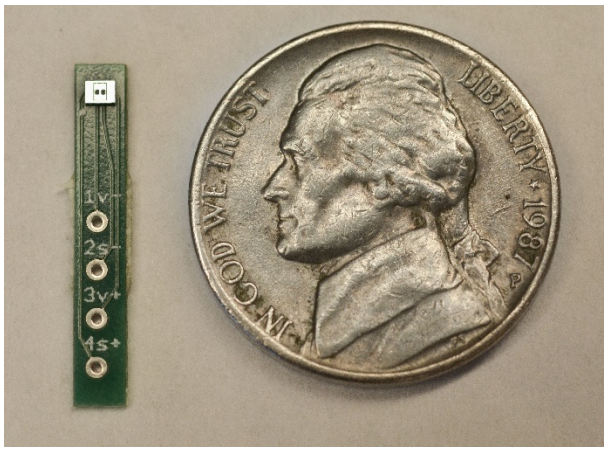

Figure 4: Custom printed circuit board with Endevco 40931 pressure sensor surface-mounted near the upper edge. Maximum assembled dimensions are 19 x 3.0 x 1.2 mm (L x W x H).

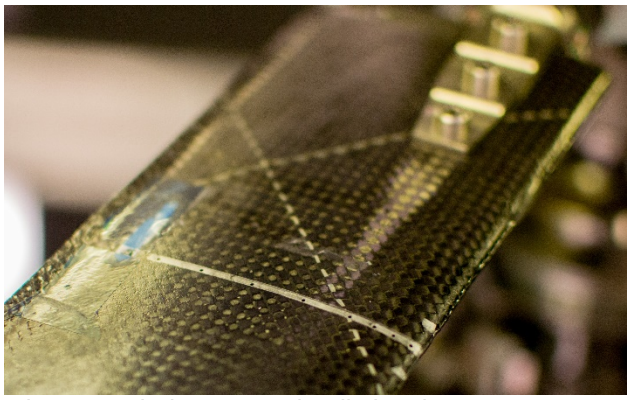

Figure 5: Blade #1 root detail showing pressure port locations (black dots on silver line) at 0.3R, upper surface.

3.1 TEST ENVELOPE

The rotor was operated at reduced rotor speeds from 40% of nominal (1000 RPM) down to 20% of nominal (450 RPM). The majority of test data was collected at 30% RPM (700 RPM). The tunnel speed varied from 30 kts to 125 kts (230 km/h). The maximum advance ratio was 1.61, a single point at zero collective, 125 kts, and 20% RPM. Collective sweeps were performed at several advance ratios, including large negative collectives at μ 1.03 and 1.21 (Figure 6). Collective sweeps at higher advance ratios were attempted, however difficulties in maintaining adequate tip path plane tracking prevented accurate trimming to zero 1p flapping. The resulting rotor thrust envelope is shown in Figure 7, and includes cases that were intentionally not trimmed to zero flapping.

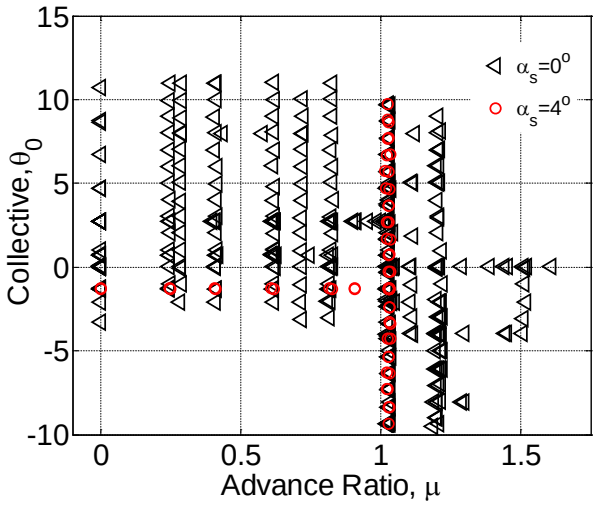

Figure 6: Collective pitch and advance ratio envelope for the wind tunnel test.

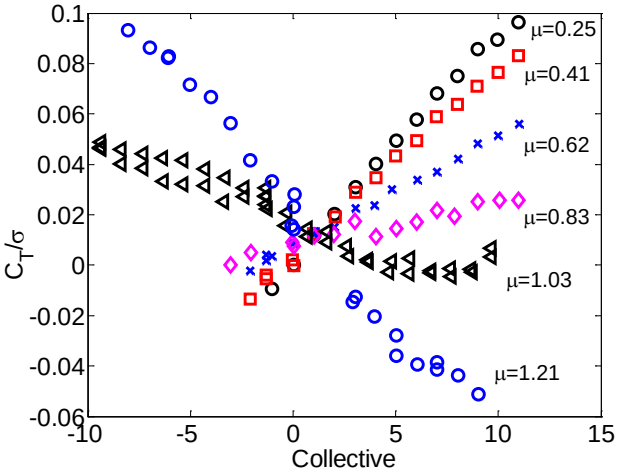

Figure 8: Thrust vs collective for varying advance ratio, $\alpha_s = 0^o$, 26% RPM for μ 1.21, 30% RPM for all other μ.

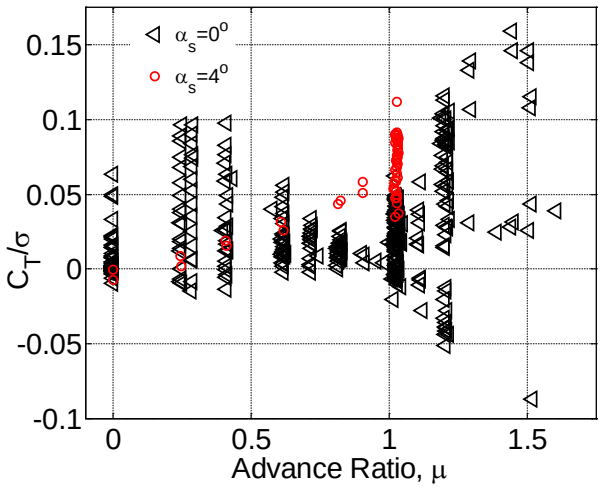

Figure 7: Rotor thrust envelope at each advance ratio.

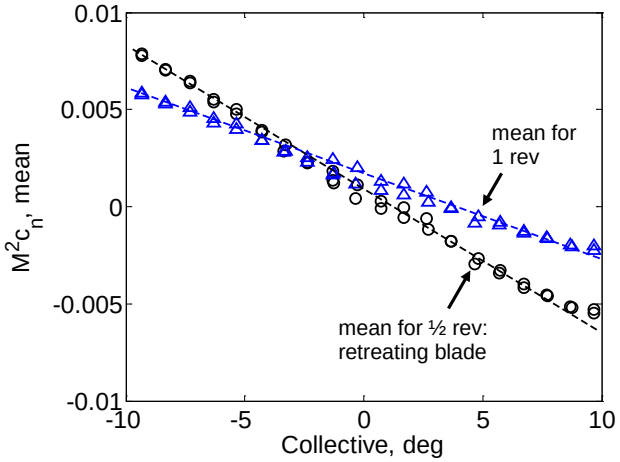

Figure 9: Mean sectional normal force at 0.3R for the retreating blade (180–360 degrees azimuth) and for the entire rotation, integrated from the blade pressure sensor data. μ = 1.03, 125 kts, $\alpha_s = 0^o$.

4. RESULTS

4.1 Performance and Control Angles

Collective sweeps were performed over a range of advance ratios to capture the progression of the collective-thrust reversal phenomenon (Figure 8). This behavior has been reported previously[1,7,11,12], but this experiment expanded the high advance ratio collective pitch range significantly. The goal was to attempt to observe non-linear behaviors predicted by analysis due to reverse-flow stall behavior[4,6,15]. No change in trends was observed for negative collectives but for collective settings beyond positive 8 degrees at μ 1.03, the thrust sensitivity does begin to turn positive. From interrogation of the 0.3R chordwise pressure sensors, the retreating blade lift production shows a slight deviation from the linear trend at the highest collectives (Figure 9), but it still has a negative slope, unlike the mean rotor thrust. The behavior of other radial stations, perhaps even further inboard, likely contribute to the overall increase in rotor thrust, but this cannot be determined from this data set.

At each condition, the rotor is trimmed to zero 1/rev flapping using swashplate cyclic pitch inputs. The longitudinal and lateral cyclic trim settings are shown in Figure 10 and Figure 11, respectively. Longitudinal cyclic shows the expected inverse linear relationship with collective, which represents the need to decrease pitch on the advancing blade and increase the pitch on the retreating blade to maintain equality of flapping. Increasing advance ratio necessitates more longitudinal cyclic input for a given collective

input, as a result of decreasing (and then reversing) flow velocity on the retreating blade. Lateral cyclic shows less sensitivity to advance ratio because there is less freestream asymmetry on the fore and aft disk. At μ of 1.21, the lateral cyclic trend flattens considerably, which could indicate the decreasing importance of the fore and aft regions of the disk for lift generation.

Rotor drag (Figure 12) shows steep increases with advance ratio, particularly at high collective settings. Plotting drag against thrust (Figure 13) shows that advance ratios between 0.83 and 1.03 generate high drag, but have low thrust capability. However, the 1.21 advance ratio cases are able to produce higher thrust levels with lower drag, due to increased reverse flow velocities on the retreating blade.

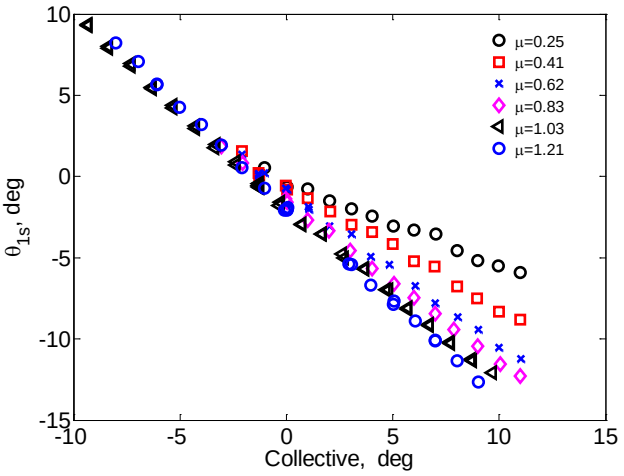

Figure 10: Longitudinal cyclic vs collective.

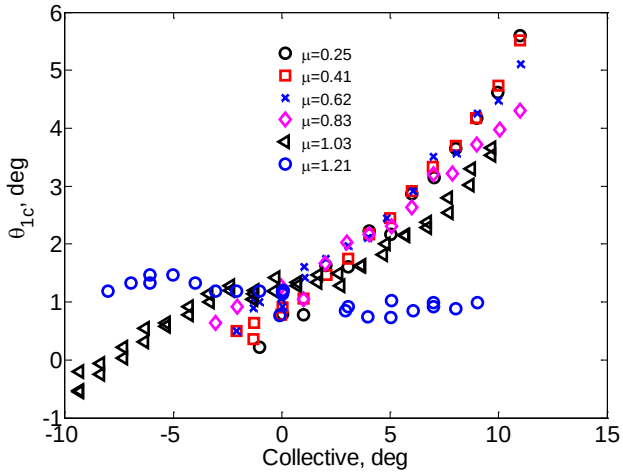

Figure 11: Lateral cyclic vs collective.

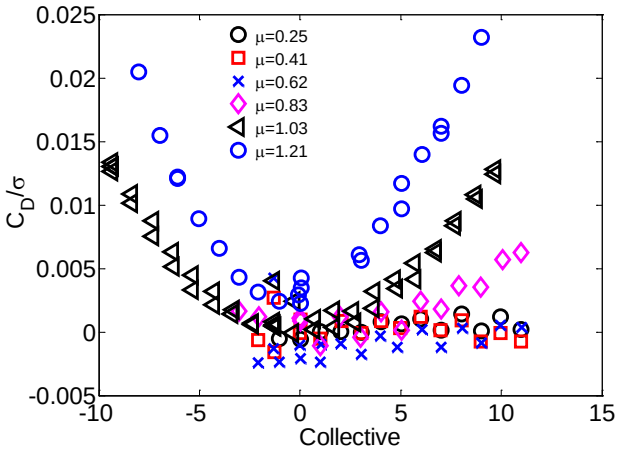

Figure 12: In-plane rotor drag (C_D=C_H) vs collective.

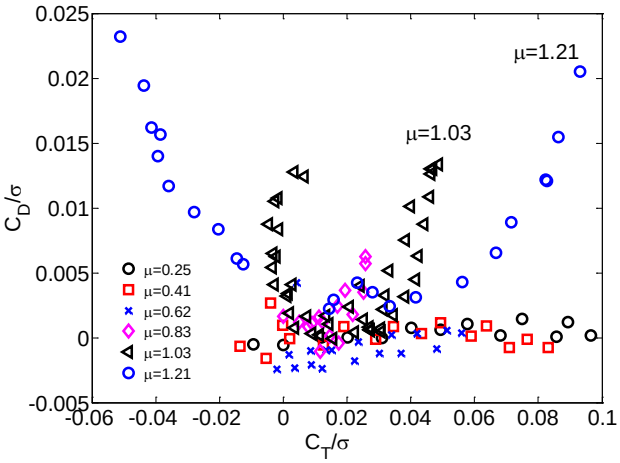

Figure 13: In-plane rotor drag (C_D=C_H) vs. rotor thrust, α_s = 0º, 26% RPM for μ 1.21, 30% RPM for all other μ.

Rotor shaft power distinctly decreases with advance ratio (Figure 14). Many cases measuring negative power, implying a state of autorotation. These are quadratic trends with collective, centered on zero degrees (symmetric airfoil). Power polars (Figure 15) show power (for a constant thrust) increasing with advance ratio up until 0.83, followed by a decrease in shaft power and autorotation at higher thrusts at μ = 1.03 and 1.21. At the negative power conditions, the rotor drag is still positive and increasing, so there is a trade between shaft power and propulsive power in this regime (Figure 16).

Shaft power and propulsive power effects can be combined into a total power metric, which can be transformed into a rotor equivalent drag force. This plotted versus thrust represents the overall performance polar for the rotor (Figure 17), and the ratio provides the lift-to-drag ratio of the rotor (Figure 18).

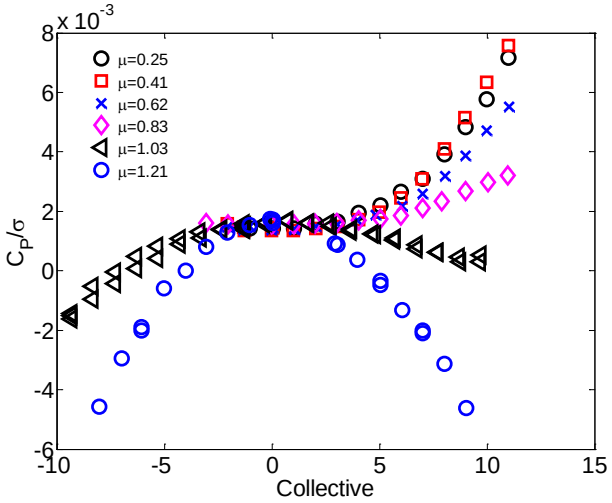

Figure 14: Power vs collective.

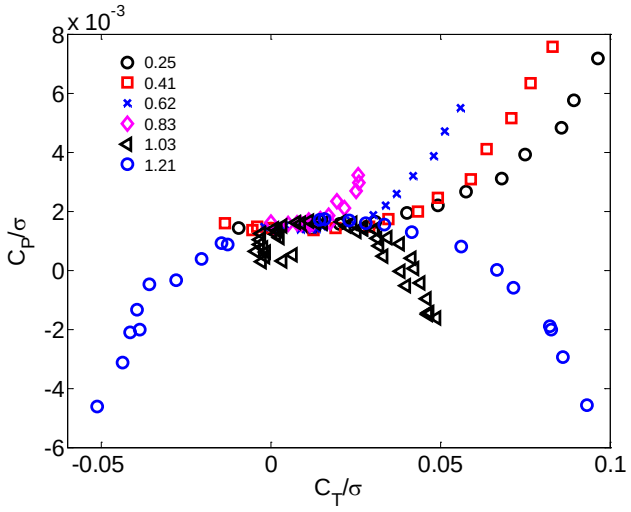

Figure 15: Power vs thrust, negative power implies autorotation.

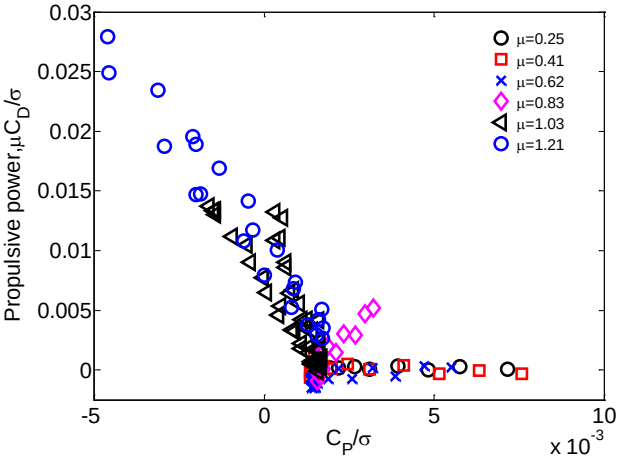

Figure 16: Propulsive power vs. shaft power.

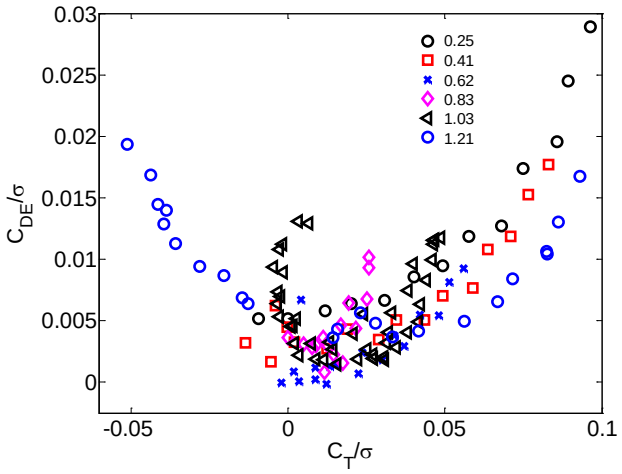

Figure 17: Rotor equivalent drag vs thrust.

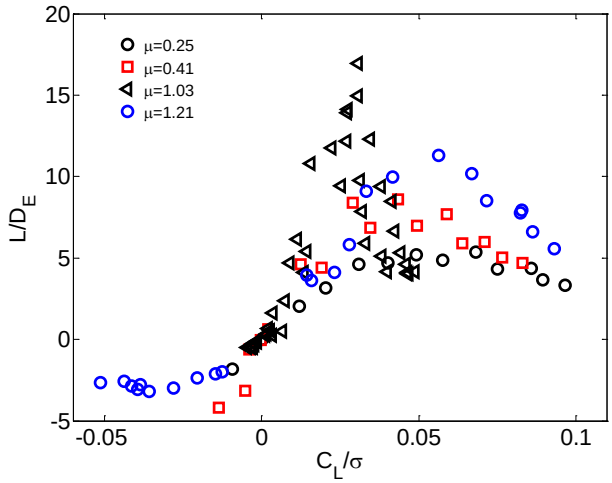

Figure 18: Rotor lift to drag ratio vs lift.

4.1 Blade Pressures and Dynamic Stall

Selected investigations into the blade pressure measurements at 0.3R are presented as representative behavior at high advance ratio. The inboard span location was chosen primarily to observe the effects of strong reverse-flow including trailing edge dynamic stall. Datta, Yeo, and Norman[9–11] observed evidence of what they termed “reverse-chord dynamic stall” in blade pressure sensor data from full-scale UH-60A slowed-rotor wind tunnel testing. The behavior is typified by a suction peak near the trailing edge that moves along the chord (in azimuthal time) to the leading edge, and produces large pitching moments. They indeed observed this behavior in select cases at μ=0.8 and μ=1.0 for the 0.225R and 0.4R span locations. The data collected during the present work expands on the advance ratio and collective pitch setting ranges and provides further evidence of this phenomenon.

The pressure data for Case 543 (1.21 advance ratio, -6 degrees collective) are plotted for the upper and lower surface in Figure 19 and Figure 20, respectively. All but the first (leading edge) sensor are shifted down by 0.02 each to aid visualization of chordwise trends. Note that positive values imply suction pressure. The rotor rotates counter-clockwise, therefore 270 degrees azimuth is the retreating blade.

In the reverse flow region on the retreating blade there is a clear passage of a suction peak over the upper surface, originating at the trailing edge and moving towards the leading edge. The blade pitch at 270 degrees azimuth ($\theta_0+\theta_{1s}$) is around -12 degrees. While not the same as angle of attack, it is likely that the blade is operating beyond the static stall limit for the sharp-edged reverse-flow airfoil.

The chordwise pressure distribution is shown at 257 degrees azimuth, where the suction pressure peak occurs at the trailing edge (Figure 21). It is clear the center of pressure has moved significantly aft on the blade chord. This dynamic stall vortex forming on the upper surface trailing edge causes a negative pitching moment which can be seen after integrating the pressure data (Figure 22). The pitching moment manifests as a negative blade torsion moment (Figure 23) and a compression force impulse in the pitch link (Figure 24) around 257–275 degrees azimuth.

This unsteady behavior, however, does produce a significant amount of lift in the third and fourth quadrants compared with the first and second (Figure 25). The retreating blade lift comes at the cost of high negative drag (towards leading edge), which subtracts from shaft power (driving torque) but adds to propulsive power.

It was shown that pitch link load amplitude can thus be indicative of the severity of reverse flow at high advance ratios. The magnitude of the ½ peak-to-peak loads vary with collective pitch (Figure 26) and are about 6 times higher at μ=1.0 compared with a conventional advance ratio of 0.25. With negative collective settings, the pitch link experiences compression (blade pitch down moment) and with positive collectives the pitch link has a positive impulse (blade pitch up moment) in reverse flow (Figure 27).

The trailing edge pressure sensor of the lower surface reveals at which positive collective setting the onset of reverse-chord dynamic stall happens at μ=1.03 (Figure 28). The trailing edge suction peak begins to form at 3.7 degrees collective, which also correlates with the collective at which the increase in pitch link amplitudes occurs (Figure 26, μ=1.03).

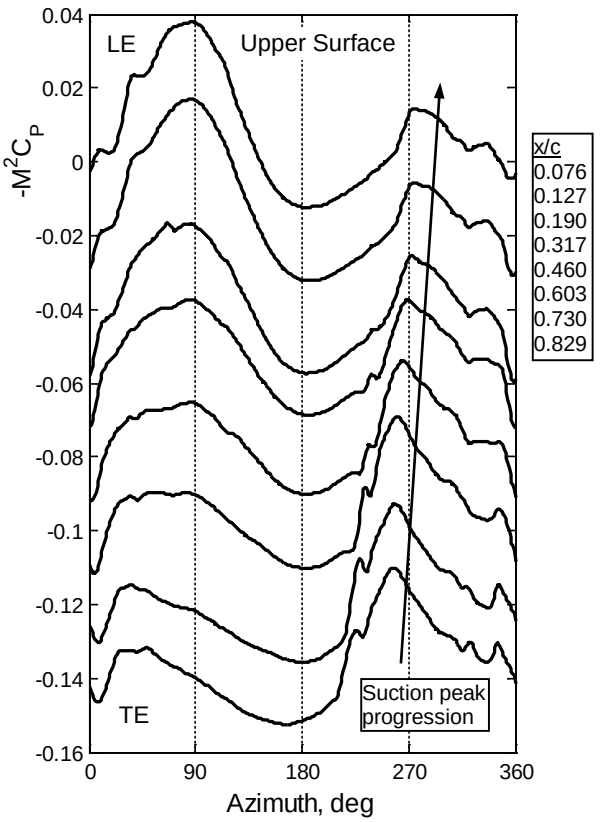

Figure 19: Upper surface blade pressure, 0.3R position, Case 543: α_s = 0°, μ = 1.21, -6° collective.

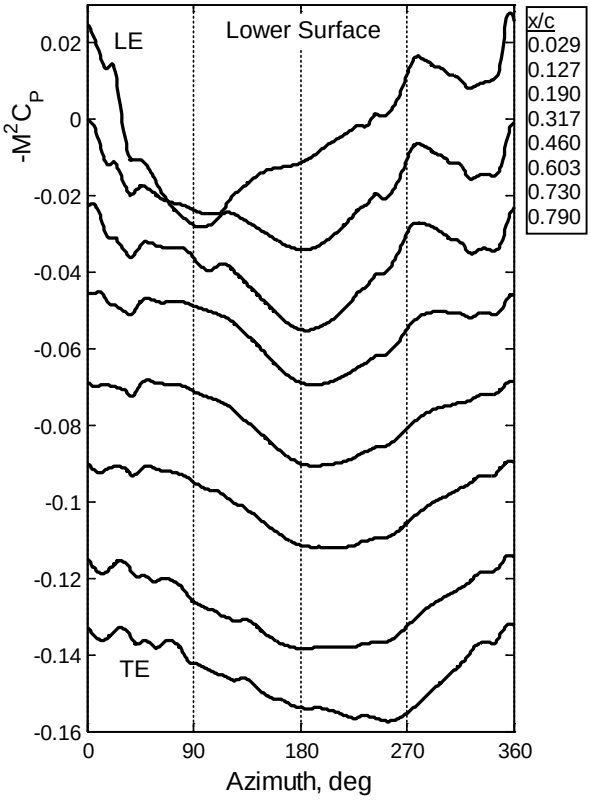

Figure 20: Lower surface blade pressure, 0.3R position, Case 543: α_s = 0°, μ = 1.21, -6° collective.

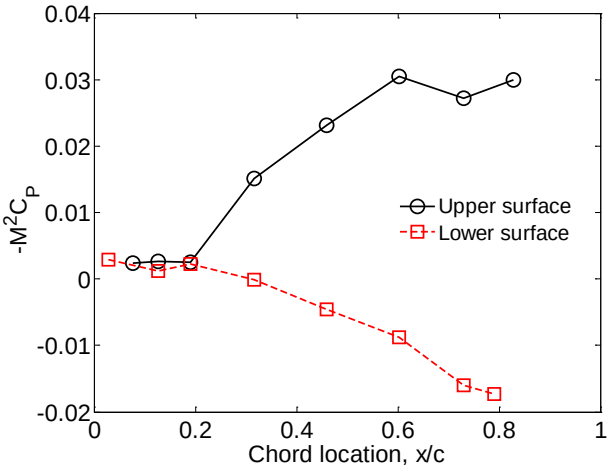

Figure 21: Chordwise pressure at 257 degrees azimuth. Case 543: $\alpha_s = 0^o$, $\mu = 1.21$, -6^o collective.

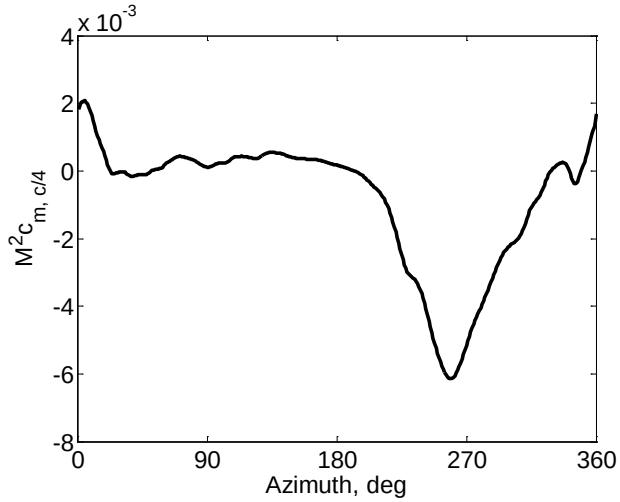

Figure 22: Pitching moment coefficient at c/4 vs. azimuth. Values integrated from pressure data. Case 543: $\alpha_s = 0^o$, $\mu = 1.21$, -6^o collective.

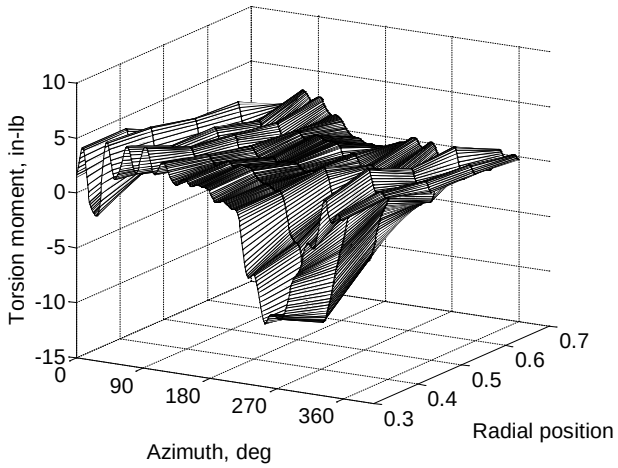

Figure 23: Measured blade torsion moment variation with azimuth and radial position. Case 543: $\alpha_s = 0^o$, $\mu = 1.21$, -6^o collective.

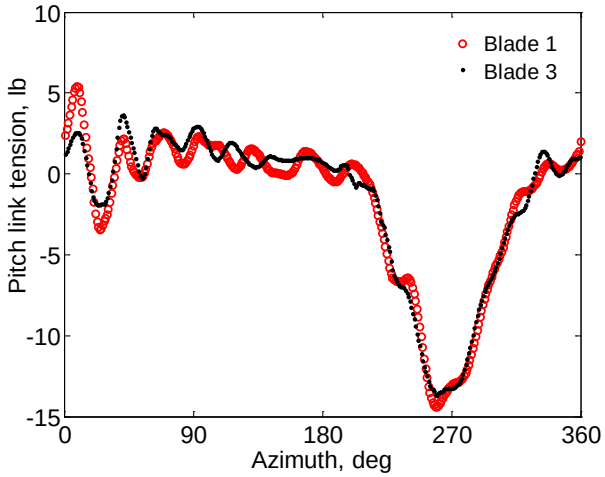

Figure 24: Pitch link load for Blade 1 and Blade 3, showing negative impulse on the retreating side. Case 543: $\alpha_s = 0^o$, $\mu = 1.21$, -6^o collective.

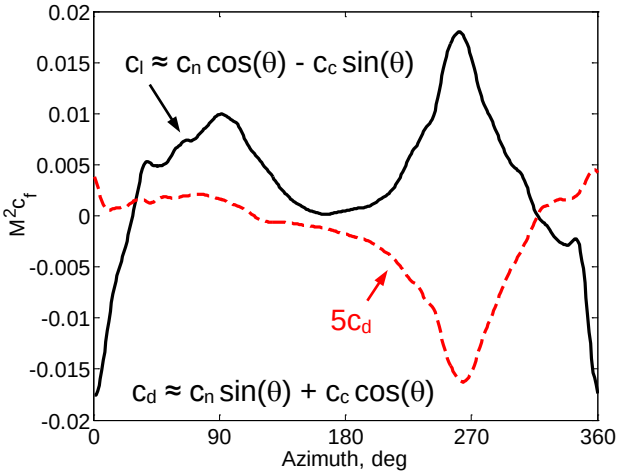

Figure 25: Lift and drag coefficients (approximate). Case 543: $\alpha_s = 0^o$, $\mu = 1.21$, -6^o collective.

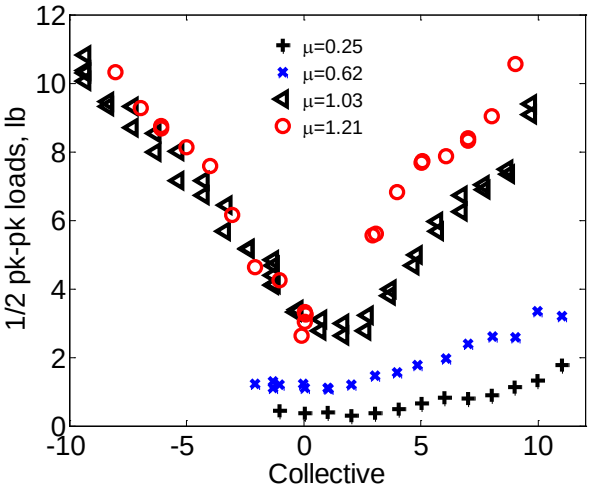

Figure 26: Pitch link load amplitude variation with collective pitch.

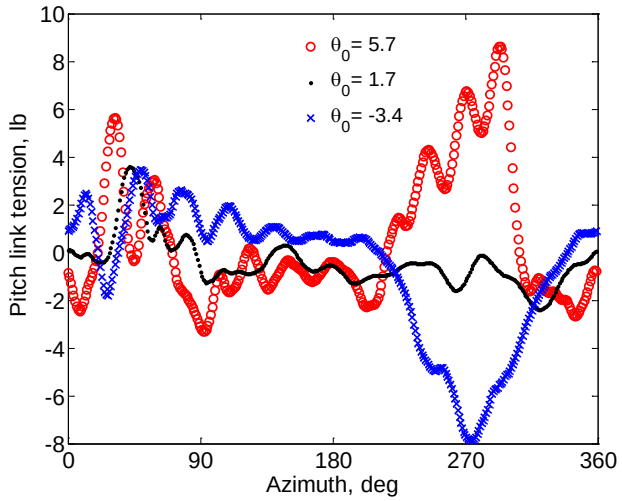

Figure 27: Pitch link load at μ=1.03 for three collective settings, showing the pitch link impulse magnitude and direction is strongly related to collective setting.

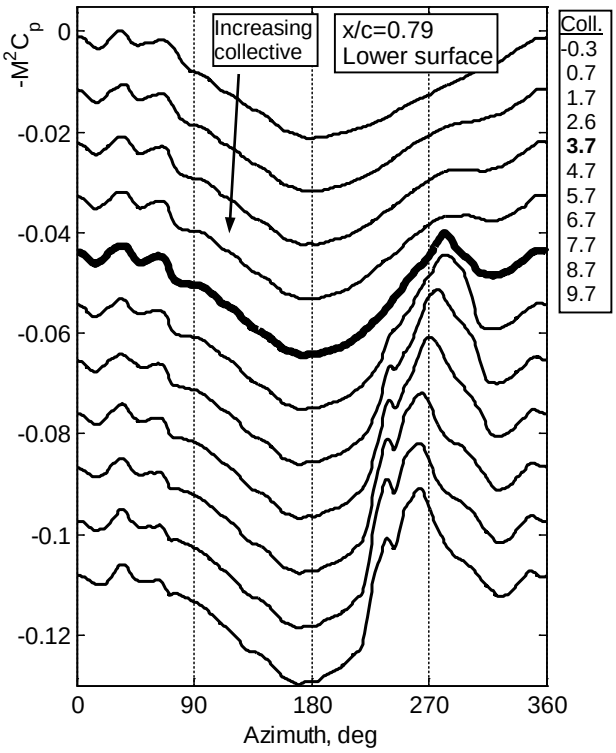

Figure 28: Pressure distribution change with increasing collective, lower surface trailing edge sensor (x/c=0.79), α_s = 0°, μ = 1.03. Thick line denotes onset of dynamic stall effects.

4.2 Vibratory Hub Loads

Vibratory hub loads were processed from the time history of the hub load-cell data, and corrected with a dynamic calibration[14]. The vertical hub loads correlated well with previous testing done by the authors with a rotor of similar geometry and testing conditions (Figure 29)[14].

The amplitude of the 4/rev hub vertical force is similar in magnitude among all advance ratios at low negative collectives (Figure 30). As collective increases, the vibratory amplitude increases rapidly for the high advance ratio cases, similarly to the pitch link loads. There is not much difference between 1.03 and 1.21 advance ratios until the highest positive collectives. When plotting against rotor thrust (Figure 31), it is clear that the 1.21 advance ratio case shows a decrease in amplitude for similar thrust levels compared to the 1.03 advance ratio cases. This reflects the improved thrust generation capability of the retreating blade at lower pitch angles (due to increased mean retreating blade velocity). The vibratory magnitude at 1.21 is still approximately 7-times higher compared to the conventional 0.25 advance ratio.

The in-plane 4/rev hub loads are shown in Figure 32 and Figure 33. Currently only the 4p in-plane hub loads at 30% RPM have been processed, which excludes the 1.21 advance ratio cases. The Fx and Fy vibratory hub loads are similar in magnitudes at low advance ratio for all collectives. At high advance ratio, the Fx (longitudinal/axial force) components increase much more steeply than the Fy (side force) components. The large retreating blade pitch required at high advance ratio is likely the cause of the 4/rev forcing in the axial direction as it would not largely effect the side force. The retreating blade drag impulse shown earlier in Figure 25 would support this hypothesis. The side force amplitude does show large percentage increases with collective, but the absolute values are low in comparison with axial and vertical force amplitudes.

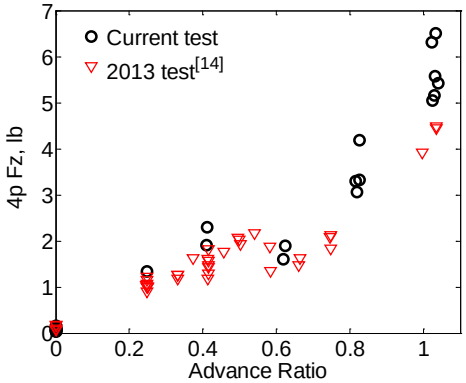

Figure 29: Vertical 4/rev vibratory hub load vs advance ratio, comparison with previous test data. α_s = 0°, θ_0 = 0°, 30% RPM.

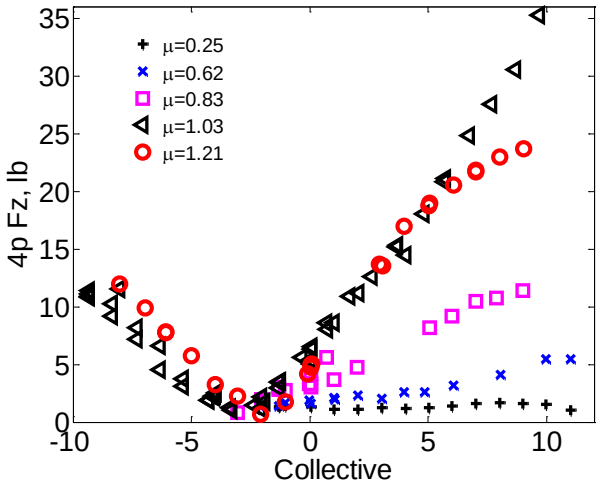

Figure 30: Vertical 4/rev vibratory hub load vs collective, 30% RPM, $\alpha_s = 0^o$.

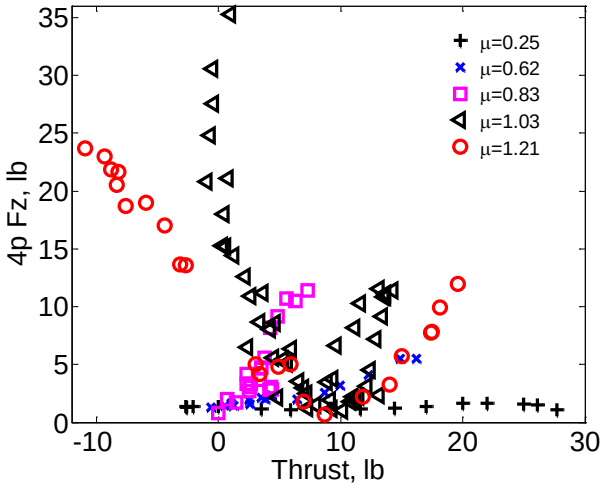

Figure 31: Vertical 4/rev vibratory hub load vs dimensional thrust, 30% RPM, $\alpha_s = 0^o$.

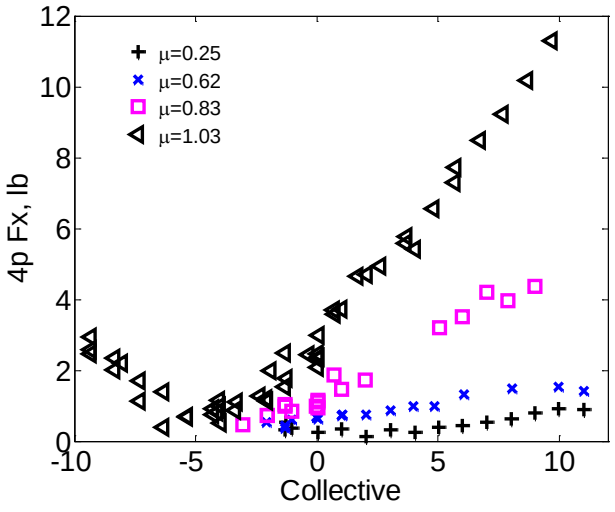

Figure 32: Longitudinal vibratory hub load vs collective, 30% RPM, $\alpha_s = 0^o$.

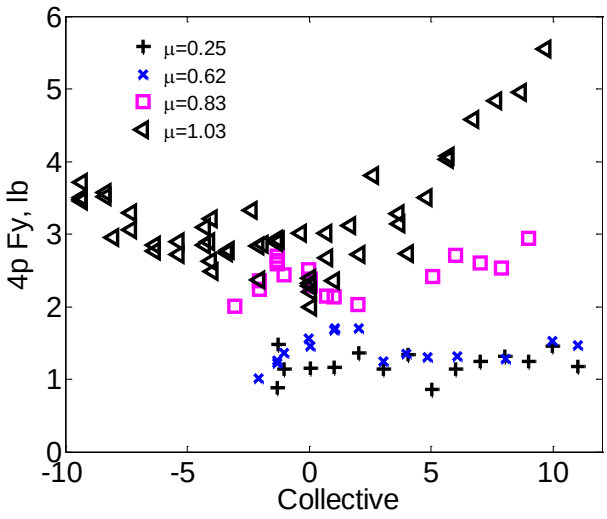

Figure 33: Lateral 4/rev vibratory hub load vs collective, 30% RPM, $\alpha_s = 0^o$.

5. CONCLUSIONS

A 1.7 meter diameter Mach-scale model rotor was tested in a wind tunnel at slowed-rotor conditions to advance ratios up to 1.61. Performance, vibratory hub loads, blade loads, and blade surface pressure measurements at 0.3R were taken. The goal was to gain insight into high-advance ratio rotor aeromechanics and provide a data set for modeling validation. The full data set is still undergoing analysis, but some selected results were reported in this paper.

Key conclusions:

1. Collective-thrust reversal was observed as expected and continued to higher positive and negative collective angles than previously measured in the literature, at μ=1.03 and μ=1.21. The mechanism of trend reversal at high positive collective was not apparent from 0.3R pressure data.
2. The thrust capability of the rotor is limited between advance ratios of about 0.8–1.0 due to reduced retreating blade mean span-wise velocity. At μ=1.21, the rotor was capable of producing larger positive thrusts by utilizing the retreating blade. The retreating blade airfoil generated lift in reverse flow, with the suction peak near the trailing edge.
3. The lifting blade in reverse flow experienced large pitching moments because of a dynamic stall vortex progressing from the trailing edge to the leading edge, producing high suction near the trailing edge, resulting in an aft center of pressure. The pitching moments were evident in the blade torsion and pitch link loads.
4. Blade loads, hub loads, and pitch link loads trended similarly with collective at high advance ratios, and appear to be mostly caused by the dynamic stall behavior in reverse flow.

6. ACKNOWLEDGEMENTS

This work was supported by the Army/Navy/NASA Vertical Lift Research Center of Excellence (VLRCOE) with Dr. Mahendra Bhagwat serving as Program Manager and Technical Monitor, grant number W911W6-11-2-0012. The authors thank graduate students Xing Wang and Anand Saxena for their assistance with rotor construction and wind tunnel testing.

7. REFERENCES

1. Jenkins, J.L., Jr., "Wind Tunnel Investigation of a Lifting Rotor Operating at Tip-Speed Ratios from 0.65 to 1.45," NASA TN-D-2628, Langley Research Center, February 1965.
2. Harris, F., "An Overview of Autogyros and The McDonnell XV-1 Convertiplane," NASA/CR-2003-212799, October 2003.
3. Harris, F., "Rotor Performance at High Advance Ratio; Theory versus Test," NASA/CR-2008-215370, October 2008.
4. Ormiston, R., "Rotor Aerodynamic Characteristics at High Advance Ratio Relevant to Compound Rotorcraft," American Helicopter Society Future Vertical Lift Aircraft Design Conference Proceedings, San Francisco, CA, January 18-20, 2012.
5. Berry, B., and Chopra, I., "Performance and Vibratory Load Measurements of a Slowed-Rotor at High Advance Ratios," American Helicopter Society 68th Annual Forum Proceedings, Fort Worth, TX, May 2012.
6. Floros, M., and Johnson, W., "Performance Analysis of the Slowed-Rotor Compound Helicopter Configuration," *Journal of the American Helicopter Society*, Volume 54, No. 2, April 2009.
7. McCloud, J., and Biggers, J., "An Investigation of Full-Scale Helicopter Rotors at High Advance Ratios and Advancing Tip Mach Numbers," NASA TN D-4632, July 1968.
8. Norman, T., Shinoda, P., Peterson, R., and Datta, A., "Full-Scale Wind Tunnel Test of the UH-60A Airloads Rotor," American Helicopter Society 67th Annual Forum Proceedings, Virginia Beach, VA, May 2011.
9. Datta, A., Yeo, H., and Norman, T., "Experimental Investigation and Fundamental Understanding of a Slowed UH-60A Rotor at High Advance Ratios," American Helicopter Society 67th Annual Forum Proceedings, Virginia Beach, VA, May 2011.
10. Datta, A., Yeo, H., and Norman, T., "Experimental Investigation and Fundamental Understanding of a Slowed UH-60A Rotor at High Advance Ratios," 37th European Rotorcraft Forum Proceedings, Gallarate, Italy, September 2011 (Revised from Ref 9).
11. Datta, A., Yeo, H., and Norman, T., "Experimental Investigation and Fundamental Understanding of a Full-Scale Slowed Rotor at High Advance Ratios," *Journal of the American Helicopter Society*, Volume 58, No. 2, April 2013 (Revised from Ref 9).
12. Berry, B. and Chopra, I., "Wind Tunnel Testing for Performance and Vibratory Loads of a Variable-Speed Mach-Scale Rotor," American Helicopter Society 67th Annual Forum Proceedings, Virginia Beach, VA, May 2011.
13. Berry, B. and Chopra, I., "High-Advance Ratio Wind Tunnel Testing of Two Mach-Scale Rotor Geometries," American Helicopter Society 69th Annual Forum Proceedings, Phoenix, AZ, May 2013.
14. Berry, B. and Chopra, I., "High Advance Ratio Wind Tunnel Testing of a Model Rotor with Pressure Measurements," Fifth Decennial AHS Aeromechanics Specialists' Conference Proceedings, San Francisco, CA, January 2014.
15. Bowen-Davies, G. and Chopra, I., "Validation of Rotor Performance and Loads at High Advance Ratio," Fifth Decennial AHS Aeromechanics Specialists' Conference Proceedings, San Francisco, CA, January 2014.

COPYRIGHT STATEMENT